Electromagnetic Losses Minimization in High-Speed Flywheel Energy Storage Systems

Andrea Floris, Alfonso Damiano, Alessandro Serpi,
Department of Electrical and Electronic Engineering,
University of Cagliari,
Cagliari, Italy,
andrea.floris86@unica.it

Abstract — This paper deals with electromagnetic loss analysis and minimization in an integrated Flywheel Energy Storage System (FESS). The FESS consists of a large-airgap Surface-Mounted Permanent Magnet Synchronous Machine (SPM), whose inner rotor integrates a carbon-fiber flywheel, leading to a compact and efficient FESS. Electromagnetic losses minimization is achieved through an accurate SPM modelling, which accounts for both Joule and core losses, as well as for flux-weakening operation. Consequently, SPM maximum efficiency is obtained by injecting a proper demagnetization current component at each operating condition, which guarantee the optimal trade-off among the different losses' contributions. The effectiveness of the proposed approach is validated through numerical simulations.

Keywords —Energy efficiency, Flux-weakening operation, Flywheel energy storage systems, Losses minimization, Permanent magnet machines, Self-discharge rate

I. INTRODUCTION

Flywheel Energy Storage Systems (FESSs) represent a very interesting solution for improving power system operation and stability, particularly their high power density and good energy density enable them to address voltage/frequency regulation and power quality issues suitably. In addition, FESSs benefit from very long lifetime and cycling capability, they are maintenance-free and environmental-friendly [1], [2]. On the other hand, FESSs are technologically complex as they include several mechanical, electromagnetic and electronic components, which require expert knowledge in different fields to design, manufacture and control [3], [4].

FESSs can be classified according to different criteria, such as their speed range (low- or high-speed) or their structure (non-integrated or integrated topology) [2], [4]. Low-speed FESSs rotate up to approximately 10 krpm, thus they are generally made of steel, guaranteeing low costs but significant volume and weight, making them suitable for large scale applications mostly [2]. High-speed FESSs, instead, present much higher maximum speeds (up to hundreds krpm), resulting in much reduced volume and weight. Consequently, they are well-suited for small-scale and vehicular applications [5]. However, the very high rotating speed requires the use of composite materials (generally epoxy carbon-fibre) as steel is not able to cope with the high mechanical stresses acting on the flywheel; this increases costs, design and manufacturing complexity [6]. Furthermore, the high-speed operating range results in very high stand-by losses and self-discharging rates, which prevent FESS to store energy for relatively long period of time (several hours); this is not a particular issue in vehicular applications, in which high-speed FESSs generally manage few amount of energy in short periods of time (few seconds/minutes), whereas it is much more critical when using high-speed FESSs for supporting renewable energy sources integration, especially photovoltaic power plants of residential users. In this regard, high-speed FESS could represent a viable alternative to battery energy storage systems for this kind of application as the latter still suffer from limited lifetime and cycling capability, as well as disposal and environmental issues [3].

In this scenario, the design and control of a high-speed FESS for residential users has been presented in [7]–[9]. In particular, the proposed FESS consists of an inner-rotor large-airgap Surface-Mounted Permanent Magnet Synchronous Machine (SPM), whose rotor integrates a carbon-fibre flywheel. The proposed FESS is able to store 8 kWh of energy within [6,18] krpm, which can be exchanged 8 kW rated power, making it competitive versus battery energy storage systems in terms of both energy and power capabilities. Although Finite Element Analyses (FEAs) and numerical simulations highlight good performance in terms of charging/discharging efficiency (approximately 96%), weak daily efficiencies are achieved (approximately 70%) due to excessive losses, especially at high-speed operations, as well as a relatively high self-discharge rate (approximately 30%).

In this context, this paper presents electromagnetic losses analysis and minimisation of the FESS proposed in [7]–[9]. An accurate modelling of the SPM is introduced at first, which enables accounting for Joule and core losses properly at different operating conditions. Based on this, the maximum efficiency control strategy is implemented, which aims at injecting an optimal demagnetizing current component to minimize the overall electromagnetic losses, even when FESS is idle, thus improving the self-discharge rate. The effectiveness of the proposed approach has been verified by comparing numerical simulation results with those presented in [7], [9], in which the demagnetizing current component is injected in accordance with flux-weakening operation needs only.

II. FESS OVERVIEW

A schematic representation of the proposed FESS is shown in Fig. 1, while its main specifications are reported in Table I. This configuration, which has been already presented in [7]–[9], consists of a ferrite-based SPM, whose inner rotor hosts a very thick carbon-fibre epoxy flywheel (approximately 36 cm wide), which acts also as a sleeve for ensuring permanent magnet containments at any speed. The flywheel is split into several concentric cylindrical layers (rims), mechanically forced to each

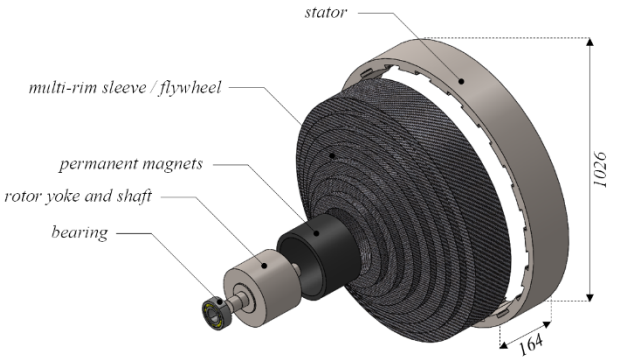

Fig. 1. view of the high-speed FESS (main dimensions expressed in mm).

TABLE I. FESS MAIN SPECIFICATIONS

Description	*symbol*	*value*	*unit*
rated power	$\hat{P}_e$	8	kW
rated torque	$\hat{T}_e$	12.7	Nm
rated speed	$\omega_{m,n}$	6	krpm
maximum speed	$\omega_{m,max}$	18	krpm
rated current	I_n	61	A
rated voltage	V_n	87	V
pole pairs	p	1	-
moment of inertia	J	18.24	kg/m^2
storable/deliverable energy	E	8	kWh
magnetic flux linkage	Λ	0.1392	Wb
phase resistance	r	47.6	mΩ
synchronous inductance	L	0.34	mH

other to ensure mechanical integrity of the overall structure. This multi-rim configuration guarantees not only to store the required high amount of energy (~9 kWh at the maximum speed of 18 krpm), but also an almost sinusoidal magnetic flux density distribution due the very large electromagnetic airgap; this is fundamental at high-speed operation to minimise system losses, especially in FESS application.

III. SPM MODELLING

The SPM modelling can be expressed by the well-known voltage, electromagnetic torque (T_e) and power (P_e) equations, which are reported in the following:

$$v_{dq} = \left(r + j\,p\omega_m L\right) i_{dq} + L\frac{di_{dq}}{dt} + j\,p\omega_m \Lambda \tag{1}$$

$$T_e = \frac{3}{2} p\Lambda\, i_q \;, \quad P_e = T_e\,\omega_m \tag{2}$$

where v_{dq} and i_{dq} denote the voltage and current space vectors in the dq synchronous reference frame, ω_m is the mechanical rotor speed, while p, r, L, and Λ are defined in Table I.

Regarding SPM operating constraints, they consist mainly of torque and power limitations (C_T and C_P, respectively), current limitation (C_i), and voltage saturation (C_v), which can be expressed as

$$\begin{aligned} &C_T: \ \left|T_e\right| \le \hat{T}_e \;, \quad C_P: \ \left|P_e\right| \le \hat{P}_e \\ &C_i: \ \left|i_{dq}\right| \le \hat{I}_p \;, \quad C_v: \ \left|v_{dq}\right| \le \frac{V_{DC}}{\sqrt{3}} \end{aligned} \tag{3}$$

where $\hat{T}_e$ and $\hat{P}_e$ denote rated electromagnetic torque and power, $\hat{I}_p$ is the peak current magnitude, and V_{DC} is the DC-link voltage.

Assuming to be at steady-state operation, substituting (1) and (2) in (3) yields

$$C_{TP}: \ \left|i_q\right| \le \hat{I}_\omega \;, \quad C_i: \ \left|i_{dq}\right| \le \hat{I}_p \;, \quad C_v: \ \left|i_{dq} - \varsigma\right| \le \rho \tag{4}$$

in which:

$$\begin{aligned} &\hat{I}_\omega = \frac{2}{3p\Lambda}\min\left\{\hat{T}_e, \frac{\hat{P}_e}{\left|\omega_m\right|}\right\}, \\ &\varsigma = -\frac{p\omega_m\Lambda\left(p\omega_m L + jr\right)}{r^2 + \left(p\omega_m L\right)^2}, \quad \rho = \frac{V_{DC}}{\sqrt{3}}\frac{1}{\sqrt{r^2 + \left(p\omega_m L\right)^2}} \end{aligned} \tag{5}$$

Based on (2) and (4), it is clear that SPM electromagnetic torque and power depend on i_q only, while i_d affects both current and voltage constraints. Consequently, suitable i_d profiles can be defined in accordance with different control strategies to ensure proper flux-weakening operation, but also additional benefits, such as maximum efficiency. In this regard, i_d is generally hold constant at zero below the rated speed as no flux-weakening is needed; this simple strategy, which is generally known as Constant Torque Angle (CTA), allows minimising the magnitude of the current space vector in accordance with (4) and, thus, Joule losses. However, it does not guarantee the maximum efficiency because core losses are not considered, which could be significant for high-speed SPM, even when operating below the rated speed [10]. Consequently, a more advanced control strategy should be employed, e.g. Maximum Efficiency (ME) [11], which determines the i_d profile to minimise the SPM overall losses based on an appropriate SPM losses modelling, which is detailed in the following subsection.

A. Losses analysis

The SPM overall losses can be classified in two categories, namely mechanical and electromagnetic losses. The mechanical losses (P_{mech}) mainly depend on the air friction in the airgap (P_{air}) and in the bearings (P_{bear}), and can be estimated in accordance with empirical methods as [12], [13]

$$P_{mech} = P_{air} + P_{bear} \tag{6}$$

$$P_{air} = \tfrac{4}{1000}\rho_a^{0.8}\beta_a^{0.2}\left(\omega_m r_r\right)^{2.8}\left(2r_r\right)^{1.8}\left(\frac{l_i}{2r_r} + 0.33\right) \tag{7}$$

$$P_{bear} = \tfrac{1}{2} n_{bear}\omega_m\,\mu F D_{bear}$$

where all the coefficients are defined in Table II. When all these parameters are set, mechanical losses depend only on rotor speed, while they are independent from SPM torque. In this regard, Fig. 2 shows the evolution of mechanical losses with the rotor speed for the proposed FESS when a vacuum containment has been assumed to reduce the air density and dynamic viscosity to the values shown in Table II.

Focusing now on electromagnetic losses, they include Joule losses in the windings (P_j) and core losses (P_{core}):

$$P_{elt} = P_j + P_{core} \,. \tag{8}$$

In particular, Joule losses can be calculated easily in accordance with the following equation:

$$P_j = \frac{3}{2} r\left(i_q^2 + i_d^2\right) \,. \tag{9}$$

TABLE II. MECHANICAL LOSSES COEFFICIENTS

Description	*symbol*	*value*	*unit*
mass density[a]	ρ_a	$20 \cdot 10^{-6}$	kg/m^3
dynamic viscosity[a]	β_a	$1.32 \cdot 10^{-3}$	Pa·s
rotor outer radius	r_r	466	mm
machine active length	l_i	164	mm
friction coefficient	μ	10^{-3}	-
number of bearings	n_{bear}	2	-
bearing load	F	1981	N
inner bearing diameter	D_{bear}	45	mm

[a.] of the fluid in the airgap

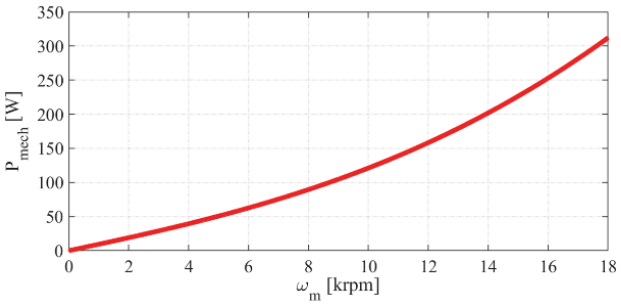

Fig. 2. Evolution of mechanical losses with the rotor speed.

Differently from mechanical losses, Joule losses are almost constant with the rotor speed, while they are proportional to the squared magnitude of the current space vector. This assumption is valid if the copper conductors chosen for the winding design are sufficiently thin, so that the skin effect can be neglected [14].

Core losses are instead generally difficult to estimate precisely. In this regard, several analytical or empirical approaches have been proposed in literature [15], [16], among which the relatively simple approach proposed in [17] for core losses estimation in permanent magnet brushless AC machine at both rated flux and flux-weakening operations. In particular, the overall core losses are estimated as

$$P_{core} = g_1\left(V_m\right) + g_2\left(V_d\right) \tag{10}$$

in which g_1 and g_2 are functions of SPM voltage at different testing conditions, namely open-circuit and short-circuit, respectively. In particular, V_m represents the magnetizing voltage, while V_d is the equivalent voltage that occurs at flux-weakening operation, based on which g_1 and g_2 are expressed as

$$\begin{aligned} g_1\left(V_m\right) &= \frac{P_{h,oc}}{E_{rms}} V_m + \frac{P_{j,oc}}{E_{rms}^2} V_m^2 + \frac{P_{ex,oc}}{E_{rms}^{1.5}} V_m^{1.5} \\ g_2\left(V_d\right) &= \frac{P_{h,sc}}{E_{rms}} V_d + \frac{P_{j,sc}}{E_{rms}^2} V_d^2 + \frac{P_{ex,sc}}{E_{rms}^{1.5}} V_d^{1.5} \end{aligned} \tag{11}$$

where the $P_{m,n}$ coefficients are related to hysteresis ($m = h$), eddy current ($m = j$), and excess losses ($m = ex$) obtained from finite element analyses at open circuit ($n = oc$) or short circuit ($n = sc$) operating conditions. Furthermore, E_{rms} represents the RMS magnitude of the back-emf, which depends on Λ and on the supply frequency f at which the analysis is carried out:

$$E_{rms} = \frac{2\pi \Lambda f}{\sqrt{2}p}, \qquad f = p\frac{\omega_m}{2\pi} \tag{12}$$

Regarding V_m and V_d, they can be computed as

$$V_d = E_{rms}\frac{i_d\sqrt{2}}{I_{sc}}, \qquad V_m = E_{rms}\sqrt{\left(1 - \frac{i_d\sqrt{2}}{I_{sc}}\right)^2 + \left(\frac{i_q\sqrt{2}}{I_{sc}}\right)^2} \tag{13}$$

where I_{sc} is determined by FEA during the short-circuit test. The latter consists of short-circuiting machine winding and making the machine to rotate at the same speed used in (12); I_{sc} is thus achieved by measuring the magnitude of any phase current at this operating condition. As a result, differently from P_{mech} and P_j, P_{core} depends on both current and speed values, as well as on the specific SPM operating condition.

B. Maximum Efficiency control strategy

The SPM overall losses can be calculated as the sum of (6) and (8), leading to

$$P_{tot} = P_{mech} + P_{elt}\,. \tag{14}$$

Consequently, P_{tot} is a function of three main variables, namely i_d, i_q, and ω_m. Consequently, since i_q is constrained directly by SPM electromagnetic torque and/or power demands, the SPM overall losses can be minimized by acting on i_d, e.g. forcing the SPM to operate in flux-weakening even when not strictly needed:

$$P_{tot,min} = \min_{i_d}\left\{P_{tot}\left(i_d, i_q, \omega_m\right)\right\}. \tag{15}$$

The ME can be implemented also in order to reduce FESS self-discharge rate. In particular, FESS self-discharge generally occurs at open circuit, i.e. $i_d = i_q = 0$, by disconnecting the SPM from its DC/AC converter [9]. As a result, FESS speed decreases due to core and frictional losses. However, ME can be employed alternatively, which means injecting suitable i_d values to reduce core losses. As this should occur at zero supply power, combining (2) and (9) yields

$$\frac{3}{2}r\left(i_q^2 + i_d^2\right) + \frac{3}{2}p\Lambda i_q\ \omega_m = 0\,. \tag{16}$$

Solving (16), i_q can be computed depending on i_d and ω_m as

$$i_q\left(i_d, \omega_m\right) = -\frac{p\Lambda i_q\ \omega_m}{2r} + \sqrt{\left(\frac{p\Lambda i_q\ \omega_m}{2r}\right)^2 - i_d^2}\,. \tag{17}$$

By substituting (17) in (15), the i_d value that minimize the overall electromagnetic losses in self-discharge mode corresponding to any ω_m can be achieved. As a result, ME implies injecting negative i_d and i_q values, which increase frictional and Joule losses, but reduce core losses more, thus improving overall self-discharging performance.

IV. RESULTS

A. FEA analysis

In order to determine the coefficients needed to evaluate the core losses through (11), FEAs have been carried out by considering the two testing mode mentioned before, namely open and short-circuit tests. Fig. 3 highlights the SPM core losses density for both cases, which are obtained at $\omega_{m,n}$ = 6 krpm. The figure reveals that core losses density is higher at open circuit test, with a maximum value of 1400 W/m^3 in the stator teeth, whereas it is very low at the short-circuit test due to significant flux-weakening operation. The losses contributions occurring at these two testing modes are reported in Table III, together with the corresponding short-circuit current value.

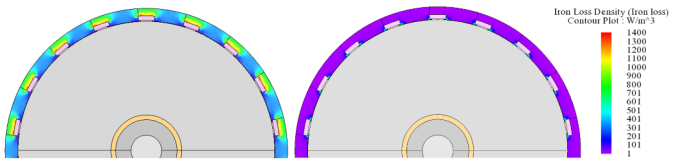

Fig. 3. FEA core losses density contour plots at open circuit (on the left) and short circuit tests (on the right) and ω_m = 6 krpm.

TABLE III. FEA PARAMETERS FOR CORE LOSSES ESTIMATION

Condition	P_h *[W]*	P_j *[W]*	P_{ex} *[W]*	i_{sc} *[A]*	ω_m *[rpm]*
open circuit	7.1	3.5	0	-	6000
short circuit	0.318	0.184	0	39.9	

B. *SPM losses and efficiency*

The effectiveness of the ME applied to the designed SPM has been verified by comparing its results to those achieved with different control strategies and/or DC-link voltage values. In particular, three different cases are considered: cases A and B consist of the well-known Maximum-Torque-Per-Ampere control strategy (MTPA) and two different DC-link voltage values (720 and 360 V), which have been already considered and compared to each other in [9], while case C consists of ME with a DC-link voltage of 720 V. which is required when connecting FESS to three-phase European 230/400 V_{RMS} 50 Hz grid. The i_d colormaps achieved on the (ω_m, T_e) plane for the three case studies are shown in Fig. 4. Focusing on case A at first, it can be seen that i_d is hold at zero at any SPM operating condition; this is due to the large DC-link voltage (720 V), which does not require flux-weakening at any speed. Differently, case B requires some i_d above 10 krpm due to the lower DC-link voltage value employed (360 V). Considering case C, i_d is always different from zero at any speed, particularly i_d increases with rotor speed to satisfy (15) and, thus, to minimize P_{tot} suitably.

Electromagnetic losses colormaps achieved for all the three cases are reported from Fig. 5 to Fig. 7, which refer to Joule losses (Fig. 5), core losses (Fig. 6) and the overall electromagnetic losses (Fig. 7). Focusing on Fig. 5 at first, it can be seen that Joule losses reach a maximum value of approximately 250 W, and they depend on electromagnetic torque mostly. This is fully valid in case A, in which no flux-weakening occurs at any speed, whereas i_d has little effects on Joule losses in both cases B and C, especially above 10 krpm. Different considerations can be made for core losses (Fig. 6), which generally decreases as flux-weakening increases. Consequently, case C exhibits the lowest core losses compare to both cases A and B, moving from a maximum value of approximately 70 W (case A) to approximately 45 W (case C). Considering now the overall electromagnetic losses achieved in the three cases (Fig. 7), some differences occur, especially at high-speed operation (beyond 13 krpm). In particular, in this operating speed region, case B exhibits lower losses than case A because i_d reduces core losses more than it increases Joule losses. This phenomenon is more significant in case C, in which ME achieves further losses minimization compared to MTPA.

In conclusion, electromagnetic efficiency maps are depicted in Fig. 8. Due to the very low losses achieved in all cases, minimal differences occur. However, it can be highlighted that case C exhibits a larger maximum efficiency region compared to cases A and B, especially at high-speed and low-torque operation. Although the efficiency improvement achieved by ME in case C could seem minimal, it should be framed in the context of the application for which the proposed system will be used; in case FESS would operate for many hours continuously, sometimes at constant speed by just delivering the torque needed for compensating for friction torque (stand-by operating mode), also a losses reduction of few tens of W could guarantee a significant improvement in terms of daily efficiency, making FESS more competitive versus battery-based solutions.

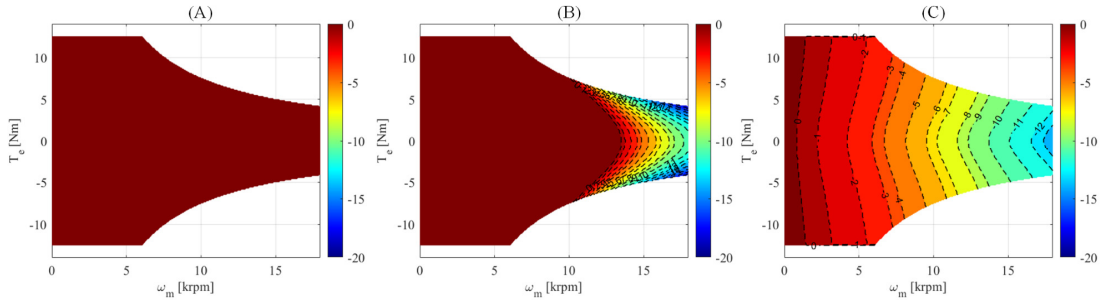

Fig. 4. The i_d map (colorbar, in A) of the SPM achieved by using different control strategies and DC-link voltages: a) MTPA with V_{DC} = 720V; b) MTPA with V_{DC} = 360V; c) ME with V_{DC} = 720V.

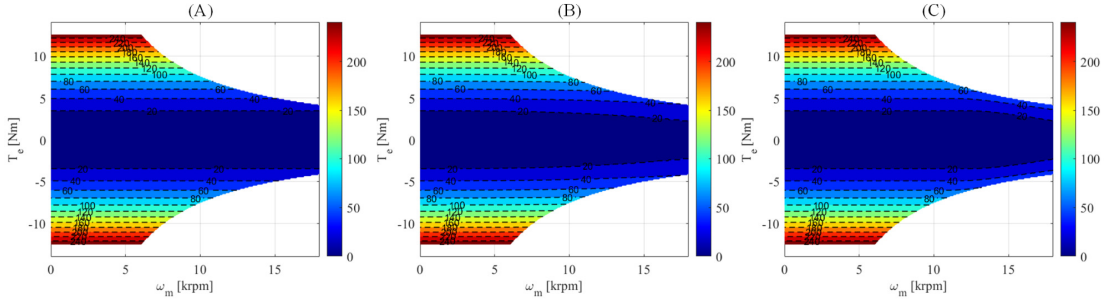

Fig. 5. Joule losses map (colorbar, in W) of the SPM achieved by using different control strategies and DC-link voltages: a) MTPA with V_{DC} = 720 V; b) MTPA with V_{DC} = 360 V; c) ME with V_{DC} = 720 V.

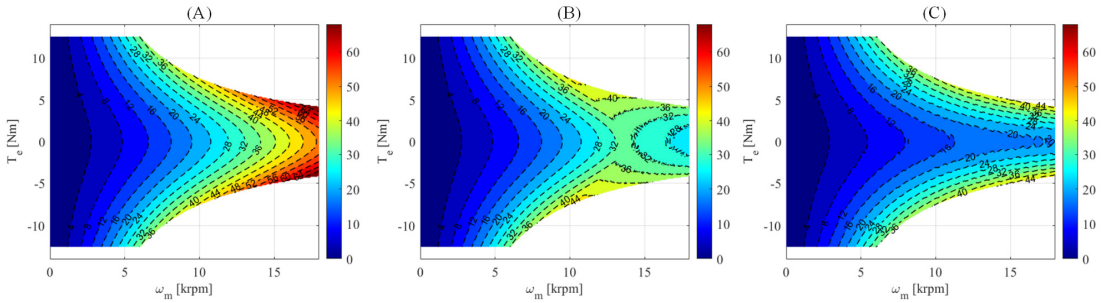

Fig. 6. Core losses map (colorbar, in W) of the SPM achieved by using different control strategies and DC-link voltages: a) MTPA with V_{DC} = 720 V; b) MTPA with V_{DC} = 360 V; c) ME with V_{DC} = 720 V.

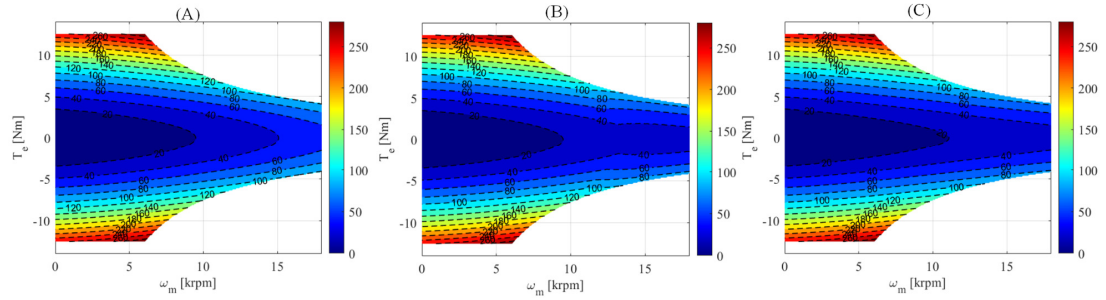

Fig. 7. Electromagnetic losses map (colorbar, in W) of the SPM achieved by using different control strategies and DC-link voltages: a) MTPA with V_{DC} = 720 V; b) MTPA with V_{DC} = 360 V; c) ME with V_{DC} = 720 V.

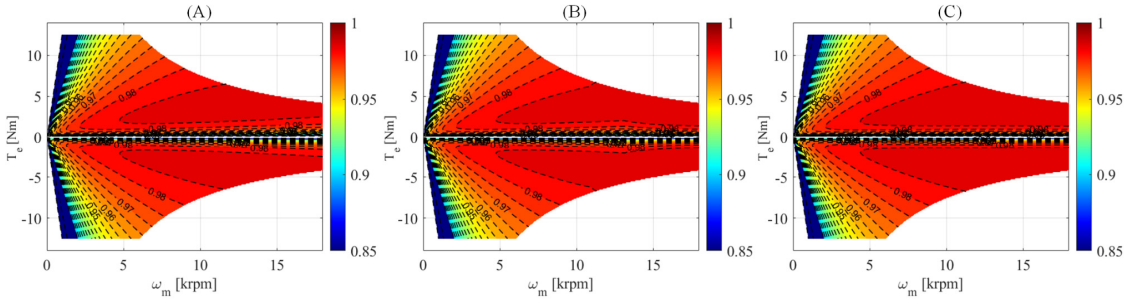

Fig. 8. Electromagnetic efficiency maps in pu of the IRLA-SPM designed considering different control strategies: a) voltage-follower PI regulator with V_{DC}=720V; b) voltage-follower PI regulator with V_{DC}=360V; c) maximum efficiency with V_{DC}=720V.

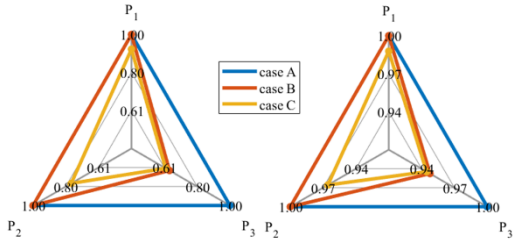

Fig. 9. Per-unit electromagnetic (on the left) and overall losses (on the right) at different stand-by operating modes and speeds.

C. *Stand-by losses and self-discharge test*

Losses reduction achievable by ME in stand-by mode is highlighted in Fig. 9, in which P_1, P_2 and P_3 represent different operating conditions achieved in stand-by mode, as summarized in Table IV. From this picture it is clear that case A exhibits the highest losses, while case C the lowest ones, with a maximum reduction of 38% on electromagnetic losses at maximum speed; since mechanical losses prevail on electromagnetic losses at high-speed operation, this losses reduction corresponds to just 6% of overall losses. However, this improvement is still significant, especially for FESS application, especially when FESS is intended to operate at high-speed for several hours. Furthermore, case B shows losses values at maximum speed comparable with case C, but slightly higher for lower speed values, behaving similarly to case A.

In conclusion, the results achieved during the self-discharge test are shown from Fig. 10 to Fig. 11 and resumed in Table V. Considering Fig. 10 at first, it is worth noting that, at open circuit mode, i_q and i_d are kept constant at zero, as expected. Differently, implementing ME, negative i_q values are injected, which introduces an additional braking torque. However, the combination of i_q and i_d obtained in this case guarantees lower overall electromagnetic losses compared to open circuit mode, as shown in Fig. 11; this results into a slightly better self-discharging rate, namely 83.0 h (28.9%) vs 81.9 h (29.3%), as highlighted in Table V.

V. Conclusion

Losses minimisation of a high-speed Surface-Mounted Permanent Magnet Synchronous Machine (SPM) has been presented in this paper. In particular, the SPM is part of an integrated Flywheel Energy Storage System (FESS), in which the flywheel acts also as a containment sleeve for the permanent magnets installed on the SPM inner rotor. It has been shown that implementing a Maximum Efficiency control strategy (ME) can

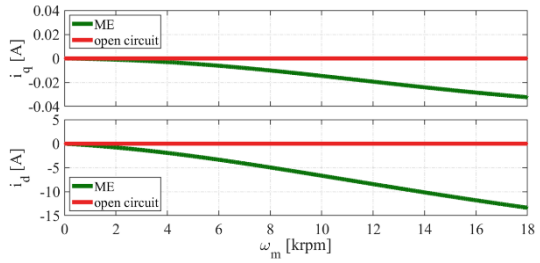

Fig. 10. The i_q and i_d evolutions with rotor speed achieved during the self-discharge test.

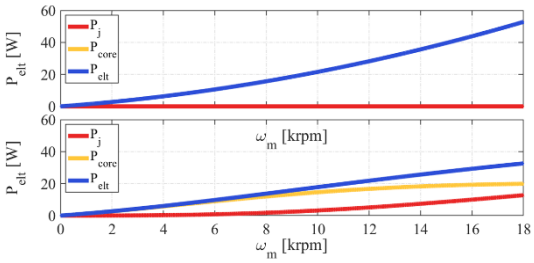

Fig. 11. Electromagnetic losses evolution with the rotor speed at self-discharge test: open circuit (on the top), and ME control strategy (on the bottom).

TABLE IV. FESS ELECTROMAGNETIC LOSSES AND OVERALL LOSSES AT DIFFERENT STAND-BY CONDITIONS

operating condition	*stand-by mode*		*electromagnetic losses [pu]*			*overall losses [pu]*		
	ω_m [krpm]	*T_e [Nm]*	*case A*	*case B*	*case C*	*case A*	*case B*	*case C*
P_1	6	0.099	1.00 (10.6 W)	1.00	0.92	1.00 (73.3 W)	1.00	0.98
P_2	12	0.126	1.00 (28.2 W)	1.00	0.77	1.00 (186.5 W)	1.00	0.96
P_3	18	0.165	1.00 (52.9 W)	0.64	0.62	1.00 (364.9 W)	0.94	0.94

TABLE V. SELF-DISCHARGE TEST RESULTS

symbol	*unit*	*$\omega_{m,nom}$*		*$\omega_{m,max}$*	
		open circuit	*ME*	*open circuit*	*ME*
i_q	A	0	$-6.1\cdot10^{-3}$	0	$-32.5\cdot10^{-3}$
i_d	A	0	–3.3	0	–13.4
P_{elt}	W	10.7	9.7	52.7	32.6
P_{mech}	W	63.3	63.3	311.9	311.9
time	h	47.2	48.3	81.9	83.0

can improve the results achieved by the more popular Maximum-Torque-Per-Ampere control strategy (MTPA), but these improvements are rather minimal (few tens of W). In any case, as long as FESS operates for long period of times at high-speed, even such a small improvement can bring detectable benefits in terms of daily efficiency, as well as stand-by and self-discharge operating modes. However, as far as FESS efficiency improvement is concerned, much more attention should be devoted to mechanical losses minimization, which are quite relevant. All these aspects will be evaluated in future works, including the prototyping stage for experimental validation.

ACKNOWLEDGMENT

This work has been developed within the project KINITIKI, which has been funded by the Sardinian Regional Government through Sardegna Ricerche under the Grant Agreement no. 1C-170 (Aids to R&D projects, POR FESR 2014-2020, Action 1.1.3).

REFERENCES

[1] P. Yulong, A. Cavagnino, S. Vaschetto, C. Feng, and A. Tenconi, 'Flywheel energy storage systems for power systems application', in *Proc. of 6th International Conference on Clean Electrical Power (ICCEP 2017)*, Jun. 2017, pp. 492–501.

[2] A. A. K. Arani, H. Karami, G. B. Gharehpetian, and M. S. A. Hejazi, 'Review of Flywheel Energy Storage Systems structures and applications in power systems and microgrids', *Renewable and Sustainable Energy Reviews*, vol. 69, pp. 9–18, Mar. 2017.

[3] S. Wicki and E. G. Hansen, 'Clean energy storage technology in the making: An innovation systems perspective on flywheel energy storage', *Journal of Cleaner Production*, vol. 162, pp. 1118–1134, Sep. 2017.

[4] F. Nadeem, S. M. S. Hussain, P. K. Tiwari, A. K. Goswami, and T. S. Ustun, 'Comparative Review of Energy Storage Systems, Their Roles, and Impacts on Future Power Systems', *IEEE Access*, vol. 7, pp. 4555–4585, 2019.

[5] M. Hedlund, J. Lundin, J. De Santiago, J. Abrahamsson, and H. Bernhoff, 'Flywheel Energy Storage for Automotive Applications', *Energies*, vol. 8, no. 10, Art. no. 10, Oct. 2015.

[6] S. J. Kim, K. Hayat, S. U. Nasir, and S. K. Ha, 'Design and fabrication of hybrid composite hubs for a multi-rim flywheel energy storage system', *Composite Structures*, vol. 107, pp. 19–29, Jan. 2014.

[7] A. Floris, A. Damiano, and A. Serpi, 'Design and Performance Assessment of an Integrated Flywheel Energy Storage Systems based on an Inner-Rotor Large-Airgap SPM', in *2020 International Conference on Electrical Machines (ICEM)*, Aug. 2020, vol. 1, pp. 633–639.

[8] A. Floris, M. Paderi, A. Damiano, F. Aymerich, and A. Serpi, 'Design criteria and methodology of a Multi-Rim Carbon-fibre Flywheel to be integrated within a Large-Airgap PMSM', in *IECON 2020 The 46th Annual Conference of the IEEE Industrial Electronics Society*, Oct. 2020, pp. 913–919.

[9] A. Floris, M. Porru, A. Damiano, and A. Serpi, 'Energy Management and Control System Design of an Integrated Flywheel Energy Storage System for Residential Users', *Applied Sciences*, vol. 11, no. 10, Art. no. 10, Jan. 2021.

[10] Q. Guo, C. Zhang, L. Li, J. Zhang, and M. Wang, 'Maximum Efficiency per Torque Control of Permanent-Magnet Synchronous Machines', *Applied Sciences*, vol. 6, no. 12, Art. no. 12, Dec. 2016.

[11] R. Krishnan, *Permanent Magnet Synchronous and Brushless DC Motor Drives*. New York: CRC Press, 2010.

[12] J. Pyrhonen, T. Jokinen, and V. Hrabovcová, *Design of rotating electrical machines*. Chichester, West Sussex, United Kingdom ; Hoboken, NJ: Wiley, 2008.

[13] D. R. Aitchison, M. Cirrincione, and N. Leijtens, 'Design development of a flywheel energy storage system for isolated Pacific Island communities', in *Proc. of 2016 IEEE International Conference on Advanced Intelligent Mechatronics (AIM)*, Jul. 2016, pp. 1628–1633.

[14] F. Magnussen and C. Sadarangani, 'Winding factors and Joule losses of permanent magnet machines with concentrated windings', in *IEEE International Electric Machines and Drives Conference, 2003. IEMDC'03.*, Jun. 2003, vol. 1, pp. 333–339 vol.1.

[15] G. Bertotti, 'General properties of power losses in soft ferromagnetic materials', *IEEE Transactions on Magnetics*, vol. 24, no. 1, pp. 621–630, Jan. 1988.

[16] K. Venkatachalam, C. R. Sullivan, T. Abdallah, and H. Tacca, 'Accurate prediction of ferrite core loss with nonsinusoidal waveforms using only Steinmetz parameters', in *COMPEL 2002. IEEE Workshop on Computers in Power Electronics.*, Mayaguez, Puerto Rico, 2002, pp. 36–41.

[17] P. H. Mellor, R. Wrobel, and D. Holliday, 'A computationally efficient iron loss model for brushless AC machines that caters for rated flux and field weakened operation', in *2009 IEEE International Electric Machines and Drives Conference*, May 2009, pp. 490–494.